Small-angle neutron scattering investigation of γ' precipitate morphology evolution in creep-exposed single-crystal Ni-base superalloy CMSX-4

2008 J. Phys.: Condens. Matter 20 104261

(http://iopscience.iop.org/0953-8984/20/10/104261)

J. Phys.: Condens. Matter **20** (2008) 104261 (8pp) doi:10.1088/0953-8984/20/10/104261

Small-angle neutron scattering investigation of γ' precipitate morphology evolution in creep-exposed single-crystal Ni-base superalloy CMSX-4

J Zrník[1], P Strunz[2], M Maldini[3], A Wiedenmann[4] and V Davydov[5]

[1] TU Košice, Letná 9, 420 00 Košice, Slovak Republic
[2] Research Centre Řež, CZ-25068 Řež near Prague, Czech Republic
[3] CNR-IENI, Via Cozzi 53, 20125 Milano, Italy
[4] HMI Berlin, Glienickerstrasse 100, D-14109 Berlin, Germany
[5] Nuclear Physics Institute, CZ-25068 Řež near Prague, Czech Republic

E-mail: strunz@ujf.cas.cz

Received 16 July 2007, in final form 2 November 2007
Published 19 February 2008
Online at stacks.iop.org/JPhysCM/20/104261

Abstract

In order to assess the material degradation of exposed gas turbine high temperature components, the creep degraded CMSX-4 single-crystal nickel-base superalloy with two axial orientations [001] and [111] was investigated. Constant load creep tests were conducted in the stress/temperature ranges of 250–780 MPa/750–950 °C resulting in rupture time variation from 50 to 4000 h. A combination of scanning electron microscopy and a non-destructive small-angle neutron scattering method (SANS) was used to investigate the directional coarsening (rafting) of the γ' precipitates in relation to the stress and temperature applied as well as to the initial crystallographic orientation of the specimens. The SANS results are discussed in terms of the correlation with the raft development, the axial orientation of specimen, the creep parameters and the mechanical properties.

(Some figures in this article are in colour only in the electronic version)

1. Introduction

Nickel-base superalloys are widely used for heavy duty gas turbine buckets. For high temperature alloys, the stability of the microstructure is an important factor determining the mechanical properties under service conditions. The buckets in current advanced gas turbines are exposed to extremely high temperatures and stresses, which induce a significant material degradation and damage during service [1].

The basic microstructure of single-crystal (SC) nickel-base superalloys contains two phases—the γ matrix is hardened by small cuboidal precipitates of γ' phase. The drawback of SC superalloys is their metallurgical instability at high temperatures. The changes in their morphological characteristics are most sensitively reflected in their deformation behaviour and result usually in an acceleration of the degradation process [2, 3]. In these alloys, the morphological evolution of the γ' precipitates at high temperatures may be considerably altered by the application of a (uniaxial) external stress [4]. Under high temperature creep conditions, the γ/γ' microstructure first becomes rafted, then slowly coarsens and becomes irregular [5–8]. This phenomenon, known as directional coarsening or 'rafting', corresponds to a breaking of the overall cubic symmetry of the precipitate shape and results in the formation of large plates, or long rods or platelets, perpendicular to the stress direction. The extent of degradation in the microstructure degrades the mechanical properties of SC superalloys and depends on the exposure temperature, time of exposure and to a lesser extent on the applied stress. The mechanical parameters of single-crystal superalloys also seem to depend on the load-axis orientation with respect to the crystallographic directions.

To check the response of the structural parameters especially to the applied load at elevated temperatures,

destructive and non-destructive testing can be used. Small-angle neutron scattering (SANS) [9, 10] proved to be an important non-destructive tool for the assessment of the microstructure of alloys. The effect of rafting on the neutron scattering pattern has been demonstrated in earlier studies which employed this bulk-sensitive technique [11, 12]. To assess the morphological changes responsible for or connected with the orientation dependence of mechanical parameters, SANS can be used together with the local information obtained by SEM.

The aim of this study was an assessment of the morphological changes corresponding to the observed dependence of mechanical properties (strain to rupture and time to fracture) on mutual crystallographic and load direction orientation in creep-exposed single-crystal superalloy CMSX-4. The investigation was performed by means of a combination of two complementary techniques, electron microscopy and SANS.

2. Experimental details

The single-crystal superalloy CMSX-4 has an outstanding combination of high temperature strength and corrosion resistance. The composition of the alloy in mass% is as follows: 9.7 Co, 6.5 Cr, 0.6 Mo, 6.4 W, 5.7 Al, 1 Ti, 0.1 Hf, 6.5 Ta, 3 Re, the balance being nickel. The alloy was provided in the form of cylindrical bars with [001] and [111] dendritic growth direction. All the bars used in this experiment had the above mentioned crystallographic direction oriented within 10° around the longitudinal axis of the bar for both growth directions. The bars were standardly heat treated. First, they were held for 1 h at 1300 °C; this was followed by a 5 h hold at the solution temperature of 1320 °C and then air cooling. Two-step ageing treatment (1100 °C for 4 h, followed by air cooling, then 870 °C for 20 h, followed by air cooling) was performed.

The microstructure of the heat treated SC specimens (figure 1) was then examined with the scanning electron microscope (SEM) JSM 6380. For this microscope, the voltage can be varied in the range of 0.5–30 kV. The microstructure study was carried out at the high resolution mode HV10 with the resolution equal to 20 nm. Samples for SEM observation were metallographically prepared and etched. SEM observations on the creep-exposed superalloy were performed on specimens cut parallel to the crystallographic direction (specimen axis) of [001] or [111].

The specimens for the creep rupture tests (gauge length of 60 mm, diameter of 6 mm) for both orientations were machined from the heat treated SC bars. The constant load creep tests were performed until rupture. The creep test conditions are stated in table 1. One sample for each particular creep condition was tested.

CMSX-4 was investigated using SANS after various loadings (temperature, stress) and at two orientations of the load axis mentioned above. An Euler cradle (for adjustment of ω, χ and ψ angles) was used to set the samples to several special orientations. The neutron scattering measurements were carried out on the V4 instrument of BENSC at the Hahn-Meitner Institute, Berlin (HMI), Germany [13].

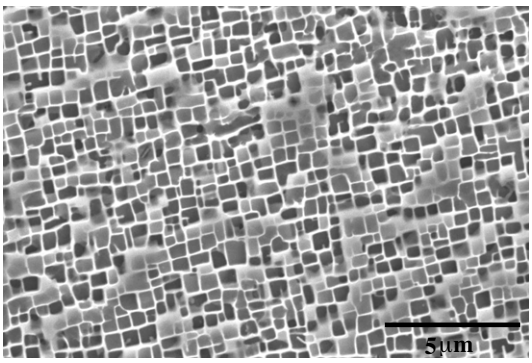

Figure 1. SEM micrograph of CMSX-4 after standard heat treatment.

The scattering data were collected at several geometries. However, the one used for the anisotropic data evaluation was: sample-to-detector distance 16 m and the neutron wavelength $\lambda = 7.5$ Å (in order to avoid a multiple Bragg scattering at certain sample orientations). The covered range of the scattering vector magnitude $Q = |\mathbf{Q}|$ was approximately 3×10^{-3}–0.02 Å^{-1} (i.e. 3×10^{-2} nm$^{-1} < Q < 0.2$ nm^{-1}), where the magnitude $Q = |\mathbf{Q}| = |\mathbf{k} - \mathbf{k}_0|$ ($\mathbf{k}_0$, $\mathbf{k}$ being the wavevectors of the incident and scattered neutrons, respectively, and $|\mathbf{k}| = |\mathbf{k}_0| = 2\pi/\lambda$). The measured raw data were corrected for background scattering and calibrated to absolute scale using the measurement of the attenuated primary beam [14]. Correction for efficiency and solid angle of the individual pixels of the 2D detector was also performed.

3. Results

3.1. Mechanical tests

The specimens of the single-crystal superalloy CMSX-4 were subjected to various tensile creep stresses at different temperatures and they showed a different deformation behaviour with regard to the strain to rupture and the lifetime for two load-axis orientations of [001] and [111]. The creep data for different strains and testing temperatures are presented in table 1. The obtained creep results are in a good agreement with results obtained for CMSX-4 SC superalloy [15]. As shown in figure 2, the time to rupture is significantly larger for the [100] load axis for the low temperatures and high stresses. On the other hand, the time to rupture is much larger for the [111] exposure when the sample undergoes deformation at a relatively high temperature and low stress.

3.2. SEM

The microstructure of SC superalloy after standard heat treatment, which is composed of γ matrix and γ' phase, is documented in figure 1. The cuboidal precipitates are arranged uniformly through the γ matrix. The average edge length of the cuboidal γ' precipitate is about 0.5 μm. The volume fraction of γ' is over 60%.

The SEM micrographs of the creep-exposed specimens for the various creep conditions (stated in table 1) are presented in

Table 1. Experimental creep conditions and results.

Sample	Load axis	Temp. (°C)	Nominal stress (MPa)	Time to rupture (h)	Creep strain to rupture	Morphology determined by SANS and SEM
C397h	[001]	—	—	—	—	—
C397	[001]	750	780	1000	15	No rafting
D431	[001]	900	500	100	21	Partial rafting
E430	[001]	900	300	2000	27	Rafted
E415	[001]	950	250	500	30	Rafted
B398h	[111]	—	—	—	—	—
B398	[111]	750	780	500	22	No rafting
C404	[111]	900	500	50	22	Partial rafting
E451	[111]	900	300	4000	20	Rafted
A396	[111]	950	250	2000	20	Rafted

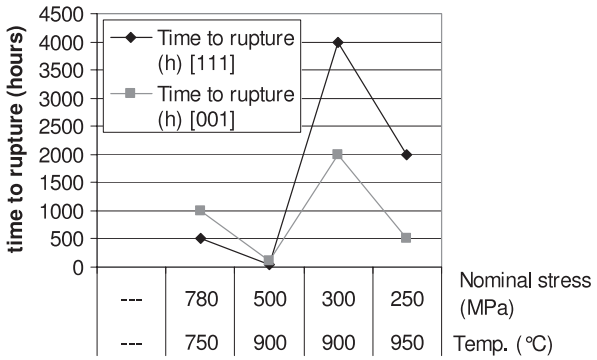

Figure 2. The time to rupture dependences for the different stresses and creep temperatures.

figure 3(a) for the [001] axis orientation and figure 3(b) for the [111] axis orientation.

Generally, for both load-axis orientations, the specimens exposed at the lower temperature of 750 °C and at higher stress showed no rafting. The specimens exposed at the higher temperature of 900 °C and medium stress of 500 MPa showed partial rafting. The other specimens exposed at 900 °C/300 MPa as well as at 950 °C/250 MPa exhibited full rafting. A quantitative comparison of [111] and [001] creep-exposed specimens considering the start of raft formation shows no striking differences, although variations in γ' morphology were observed, as shown in figure 3.

3.3. SANS

The measured and fitted 2D data are displayed in figures 4 and 5 for the selected samples and orientations. Each sample was measured in altogether nine orientations, including those with low index crystallographic directions parallel to the incoming beam as well as those without this special relation. The 2D anisotropic data for all nine orientations of a given sample were fitted at once in order to take into account the strong anisotropy of a 3D cross section in the reciprocal space, corresponding to the cuboidal and/or rafted shape of the precipitates. The precise orientation of the crystal lattice with respect to the sample axis and edges (ω_0, χ_0 and ψ_0 angles) was also determined by the fit. Two selected (out of nine) orientations are plotted in figures 4 and 5 for the selected samples.

4. Evaluation

4.1. Model

The measurements were evaluated by the NOC program for anisotropic SANS data treatment [16]. The analysis procedure is based on the numerical simulation of a scattering profile generated from a three-dimensional (3D) microstructural model of a particle system. The calculated profile is matched with the experimental curve by a weighted least square method in order to find the microstructural parameters which can be in principle extracted from the measured data.

In agreement with the direct-imaging technique (SEM) and with the symmetry of the SANS data at various sample orientations, ordered cuboidal or rafted particles were used as a model for the non-exposed and all the variously exposed samples. The shape of one individual particle can be varied in a simple way using only one shape parameter β [16] which is 0 for a cube or block having sharp edges and becomes >0 for a cuboidal particle. In the case when $\beta = 1$, the particle has a spherical or ellipsoidal shape. These particles compose an array resembling γ' precipitates in a superalloy using the mean distance and its variance as well as the mean size and its variance. A random-number generator is used to spread sizes and distances within the variance limits. An overlap of the precipitates is allowed in order to simulate the rafting process.

After this array is formed as a 3D map in the computer memory, it is transformed via the 3D Fourier transform to the 3D reciprocal space, forming in this way a 3D cross section array $\mathrm{d}\Sigma/\mathrm{d}\Omega(\mathbf{Q})$. Afterwards, a section along the Ewald sphere surface through $\mathrm{d}\Sigma/\mathrm{d}\Omega(\mathbf{Q})$ according to the sample orientation is performed. Additionally, an orientational distribution of the 3D modelled cross section is included, which in fact represents an orientational distribution of normals to the γ–γ' interface. This distribution is characterized by its full width in half-maximum (FWHM). This orientation distribution is mirrored onto the 2D scattering curve model by carrying out sectioning along the Ewald sphere surface in a 3D incremental loop whose centre is on the mean sample orientation. In this way, a 2D cross section for one sample

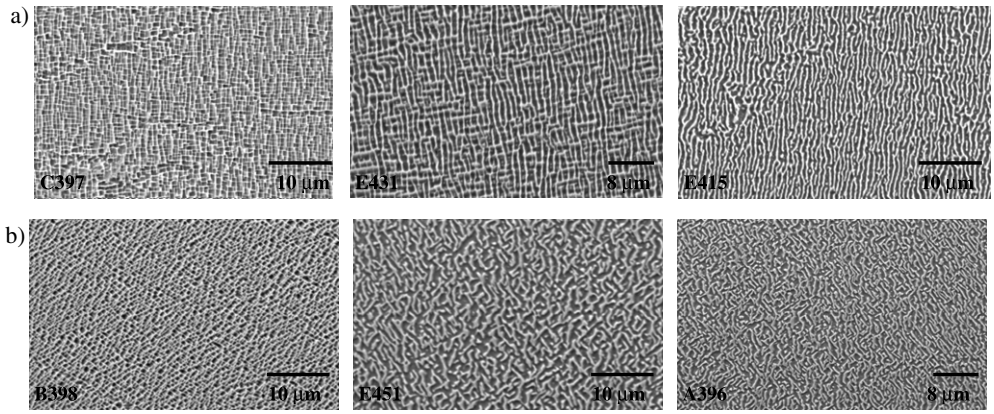

Figure 3. The SEM micrographs demonstrating the change of the γ' morphology during the creep exposure for SC specimens with axis orientation: (a) [001] and (b) [111].

orientation is received. Similarly, 2D cross sections for the other sample orientations can be obtained (sections through the same 3D cross section array).

Finally, the multiple-scattering correction and the resolution-function smearing are performed and these modelled data are compared with those measured. The procedure can be repeated in a loop with varying parameters of the model (Levenberg–Marquardt method [17]) in order to find the optimum set of parameters.

4.2. Fit

In the present case, where the precipitates in CMSX-4 after standard heat treatment are large, the measured scattering curves do not contain information on the size and distance. Therefore, the mean distance was fixed at a reasonable value. The precipitate sizes in [100] and in [001] directions could be fixed in a similar way. However, as they indirectly determine the amount of interface perpendicular to [100] and the amount of interface perpendicular to [001] (see the models in figure 4) and thus also the degree of the rafting, they were left free. A certain variation of the size and distance of the modelled particles, which can be observed in figures 4 and 5, was allowed using non-zero variances of the size and distance distributions in the preliminary fit. The size and distance variation was performed basically only in order to allow better correspondence with variations visible in the SEM micrographs.

Because the measurement was performed at nine different orientations, the representation of the 3D cross section is sufficient for refining the orientation angles ω_0, χ_0 and ψ_0 together with fitting of the microstructural parameters. The parameters which can be determined are: morphology (cuboids or rafted precipitates; their particular shape defined by β), interface orientation distribution FWHM and specific interface between γ and γ'.

The sections through 3D real-space models representing the precipitates, which match best the measured data for the selected samples, are depicted in figures 4 and 5. It should, however, be pointed out that three equivalent subsets of rafts, perpendicular to the crystallographic directions [100], [010] and [001], are in fact modelled in the case of the [111]-deformed samples (figure 5).

The criterion for satisfactorily good fit is the chi square value. Its minimum ranged from 0.75 to 1.9 for the individual samples, even though nine different orientations (i.e. nine 2D scattering patterns) were fitted at once. Taking this into account, the fit is remarkably good.

In this numerical analysis, the estimation of the statistical errors for the determined parameters can be done only by repeating the fitting cycle several times with varying input free parameters. As this is time demanding—each (in fact 3D) fit takes 6–15 h on a fast PC—a limited error analysis can be done within a reasonable time. The errors of the resulting parameters were thus calculated in this way only for some of the measured samples. Nevertheless, the relative errors for these samples represent well—highly probably—the relative errors for the others. It has to be noted that these errors mirror the statistical errors of the measurement only. They do not represent the possible imperfections of the adopted model (i.e. the simplification of the real precipitate microstructure). However, the significantly good correspondence of all the modelled SANS curves with those measured indicates that the model describes the important characteristics of the γ' precipitate microstructure as well as their trends rather well.

5. Discussion

5.1. Microstructure evolution with creep exposure

The shape parameter equals approximately 0.27 for the unexposed sample (i.e. cuboidal shape). The shape evolves towards oblate ellipsoid ($\beta = 1$) for the most loaded samples (900 °C/300 MPa and 950 °C/250 MPa). It should be noted, however, that even the lowest temperature exposure (750 °C/780 MPa) leads to the change of the shape of the cuboidal precipitates ($\beta = 0.4$) and probably also to a small elongation (<10%) of precipitates in [100] and [010] directions with respect to [001].

Among the samples with the load axis [001], the sample exposed at 750 °C with 780 MPa (time to rupture 1000 h) showed practically no rafting indication (as the scattering

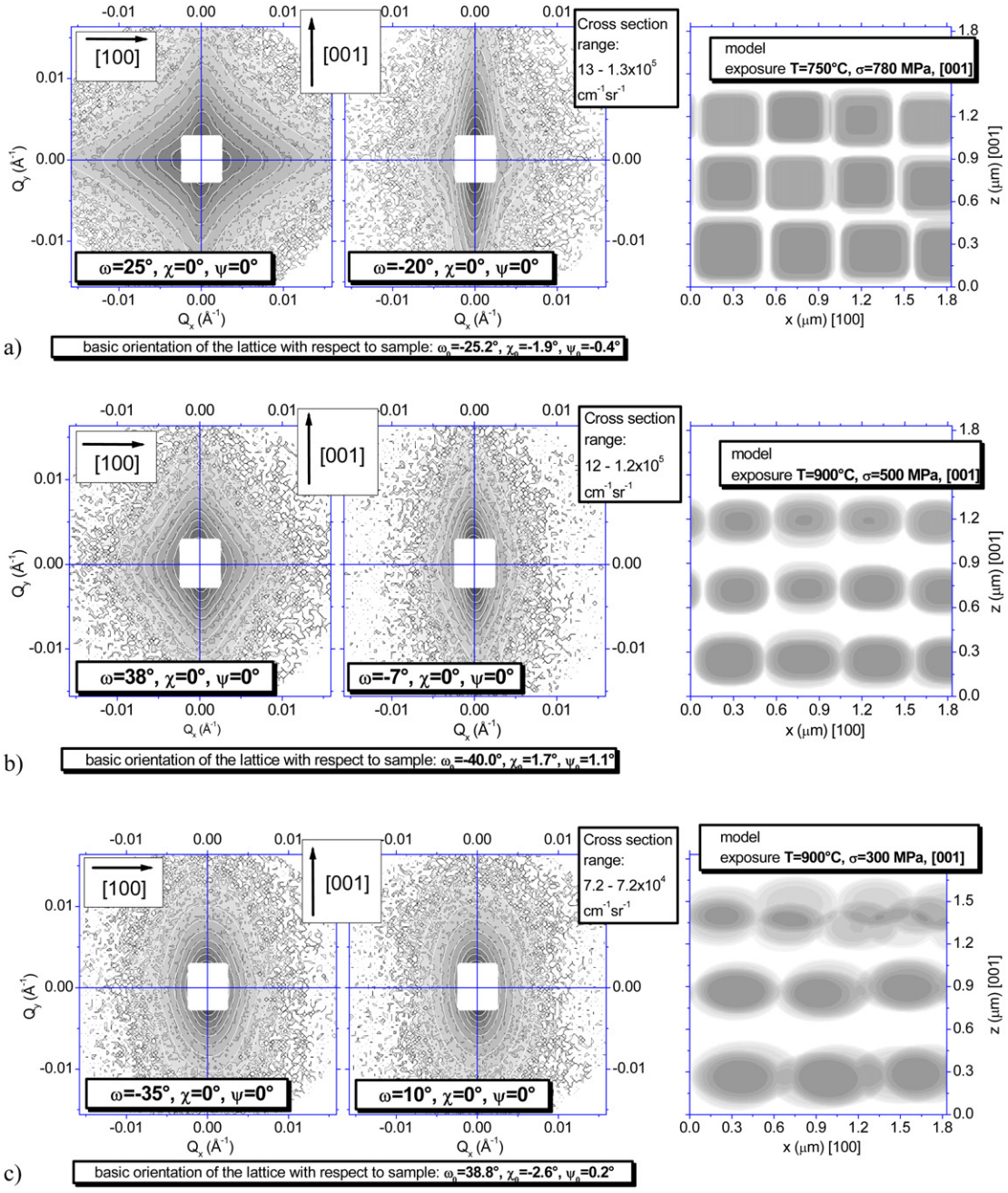

Figure 4. The selected 2D SANS patterns (differential cross section in $\mathrm{cm}^{-1}\ \mathrm{sr}^{-1}$; greyscale: measurement; white equi-intensity lines: fit; on a logarithmic scale) and the optimum model for the load axis [001]. Exposure (a) $T = 750\,^{\circ}\mathrm{C}$, $\sigma = 780$ MPa, (b) $T = 900\,^{\circ}\mathrm{C}$, $\sigma = 500$ MPa, (c) $T = 900\,^{\circ}\mathrm{C}$, $p = 300$ MPa. The size scale of the model is only indicative as the size parameters were not determined from the SANS data.

pattern has nearly fourfold symmetry when both [100] and [001] are perpendicular to the beam), except the small elongation mentioned above. The sample exposed at 900 °C with 500 MPa (100 h) clearly showed partial rafting. It can be deduced that the diffusion effects do not last long enough for forming rafts for the samples exposed at lower temperatures and higher stresses. The other two samples exposed at 900 °C with 300 MPa (2000 h) and at 950 °C (250 MPa, 500 h) exhibited a full rafting (practically no dependence of the SANS pattern on the rotation around the load axis). The rafting thus occurs only above a temperature threshold which is between 750 and 900 °C.

The estimation of the morphology of the precipitates for samples with load axis [111] is more difficult as the raft microstructure is more complex. It can be deduced that there is no raft formation with interfaces perpendicular to the stress axis (i.e. to [111]). The coarsening occurs uniformly in all three planes (100), (010) and (001). Due to this equivalence (unlike for the samples stressed along [001]), there is no change in the general character of the SANS pattern: streaks do not disappear fully in certain crystallographic directions during the rafting process, they are only more smeared for the more exposed samples. By combining SANS and SEM, similar morphology

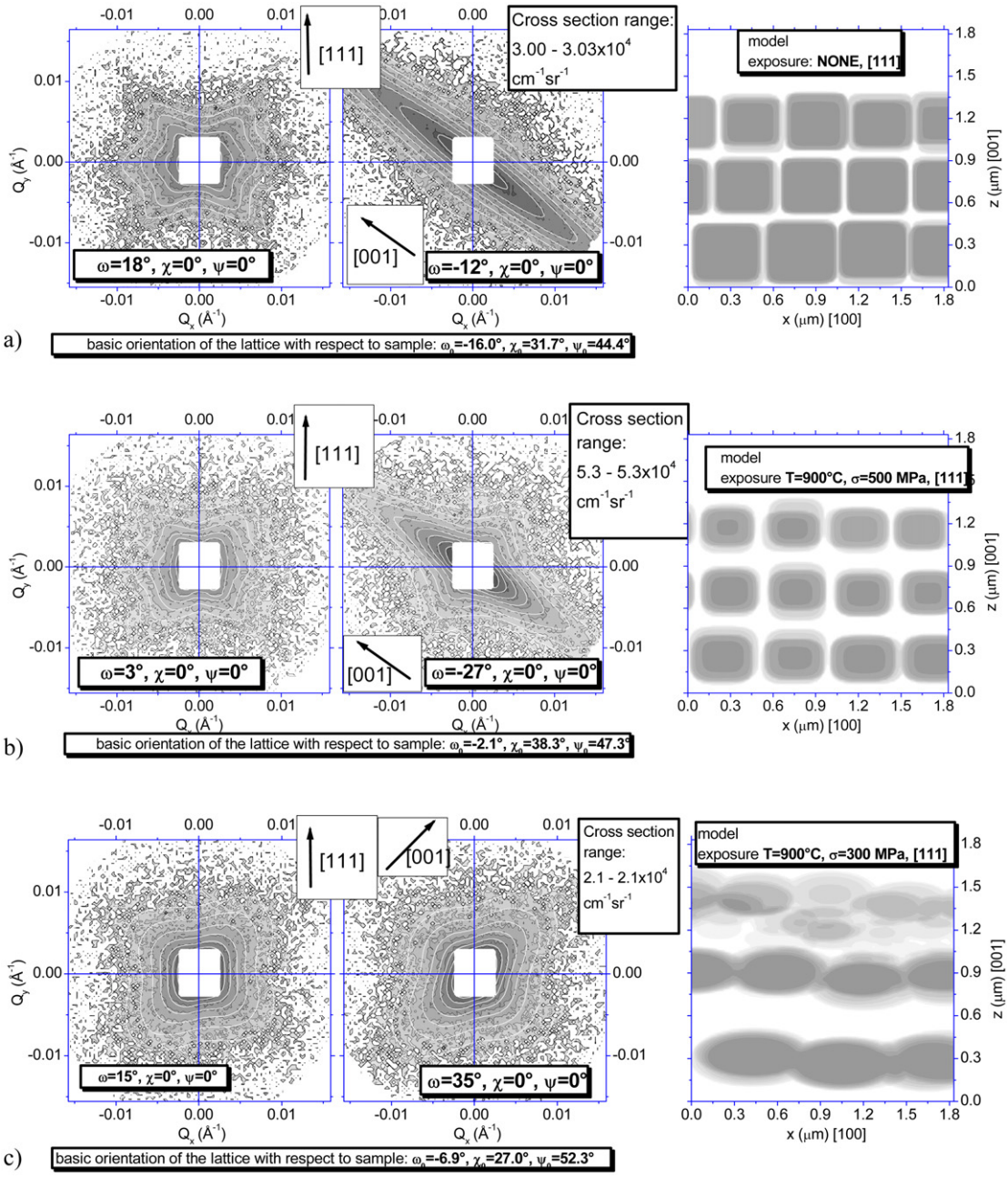

Figure 5. The selected 2D SANS patterns (greyscale: measurement; white equi-intensity lines: fit) and the optimum model for the load axis [111]. Exposure (a) none, (b) $T = 900\,^{\circ}\mathrm{C}$, $\sigma = 500$ MPa, (c) $T = 900\,^{\circ}\mathrm{C}$, $\sigma = 300$ MPa. The size scale of the model is only indicative as the size parameters were not determined from the SANS data.

to the [001]-exposed samples can be deduced (except that the morphology is equivalent for all three directions [100], [010] and [001] in the case of [111] deformation whereas it was uniaxial in the case of the samples exposed along [001]).

5.2. Interface orientation distribution

Along with the morphology change visible in the models, the microstructure was quantitatively evaluated in terms of γ–γ' interface orientation distribution.

The dependence of the FWHM of the orientation distribution on the exposure parameters is depicted in figure 6. For the [001]-exposed samples, the degree of irregularity increases with temperature and, for the same temperature, with the time to rupture (i.e. it decreases with the nominal stress). For the [111]-exposed samples, the evolution of the interface orientation distribution with temperature and stress around crystallographic directions ⟨100⟩ is qualitatively similar to what is observed in the samples exposed along [001]. Detailed evaluation (see figure 6), however, shows a significant difference in FWHM of orientation distribution evolution observed for [001]-and [111]-exposed samples.

Three equivalent subsets of rafts (perpendicular to [100], [010] and [001]) are always used for modelling in the case

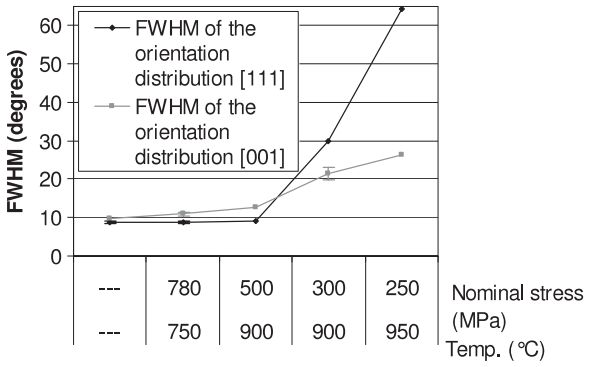

Figure 6. The dependence of the orientation distribution FWHM on the exposure parameters.

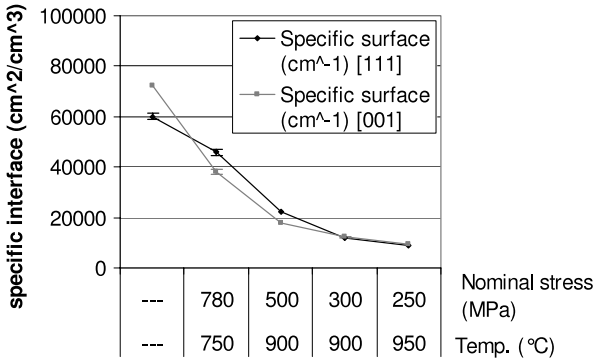

Figure 7. The dependence of the interfacial area between γ and γ' on exposure.

of [111]-deformed samples. In this case, the orientation distribution FWHM means the FWHM of the individual orientation distributions of the interface normals around these three directions ([100], [010] and [001]). FWHMs for the [001]- and the [111]-exposed samples can be thus directly compared.

5.3. Specific surface

The last parameter obtained by the fit is the specific area of the interface between γ and γ'. In order to obtain its evolution on an absolute scale, a qualified estimation of the scattering contrast has to be carried out. It can be obtained by using an estimation of the average precipitate size in a non-exposed condition (0.5 μm) from the SEM and γ' volume-fraction estimation (65%). For these values of the microstructure model, the magnitude of the cross section is fitted best when using the scattering contrast equal to 16.8×10^9 cm^{-2}. This value also corresponds well with the one obtained earlier for CMSX-4 [18]. With the help of this scattering contrast estimation, the evolution of the specific interfacial area in absolute magnitude can be plotted (figure 7).

It can be seen when comparing the non-exposed sample with the one loaded at 750 °C/780 MPa that even without rafting occurrence there is a change of the interfacial area. As no rafting occurred here, the specific interface decrease is here caused by disappearance of small precipitates from the distribution. Further decrease of the specific surface (figure 7, temperatures 900 and 950 °C) is caused by coarsening of the precipitates due to rafting, which removes some interfaces and thus lowers the specific area. The growth of the precipitates is the second cause of the strong decrease of the interfacial area.

6. Conclusions

There is no significant observable morphological difference at low temperatures and high stresses between samples loaded along [001] and [111] axes (see original and 750 °C/780 MPa as well as 900 °C/500 MPa loaded samples). There is either no (750 °C/780 MPa) or only partial (900 °C/500 MPa) rafting in these samples. Nevertheless, among these samples, the [001]-exposed ones exhibit higher time to rupture than [111] ones. It is likely that the dislocations pass through the samples loaded along [111] more easily. This is understandable as three equivalent slip-plane systems are favourably oriented in this case. SANS showed that there is no or only a very small impact of this on the γ' morphology.

On the other hand, as soon as full rafting occurs (900 °C/300 MPa and 950 °C/250 MPa loaded samples), the more favourable (from the point of view of the time to rupture) are—in turn—the [111] samples. Here, the microstructural differences between [001] and [111] samples are evident:

(a) the rafts are formed equivalently perpendicular to crystallographic directions [100], [010] and [001] in the case of [111]-deformed samples (a 'zigzag' form) whereas the rafts are exclusively perpendicular to [001] in the case of [001]-deformed samples;
(b) the orientation distribution of the interfaces between γ and γ' is much larger for [111] samples.

Most probably, both effects help to hinder the movement of dislocations and/or crack propagation and are thus responsible for the more stable microstructure of the [111]-loaded samples in the cases where rafting occurs. However, it is difficult to assess which of these two features is dominant.

Acknowledgments

The authors would like to thank BENSC (HMI Berlin) for providing the beamtime. The travel support in the frame of the 6th Framework Programme: Strengthening the European Research Area, Research Infrastructures, contract No. RII3-CT-2003-505925 (NMI3), is acknowledged as well. One of the authors (P Strunz) also acknowledges the support by MSM2672244501 project. J Zrník acknowledges the support of the Ministry of Education of the Slovak Republic (COST 538 Action project).

References

[1] Cetel A D and Duhl D N 1988 Second generation of nickel base single crystal superalloys *Superalloys 1988* ed D N Duhl *et al* (Warrendale, PA: TMS Publication) pp 253–44
[2] Brooks J W and Bridges P J 1988 *Superalloys 1988* (Warrendale, PA: TMS Publication) p 31

[3] Radawich J F 1994 *Superalloys 718, 625, 706 and Various Derivatives* (Warrendale, PA: TMS publication) p 635
[4] Chang J C and Allen S M 1999 *J. Mater. Res.* **6** 1843
[5] Pineau A 1976 *Acta Metall.* **24** 559
[6] Pollock T M and Argon A S 1994 *Acta Metall. Mater.* **42** 1895
[7] Tien J K and Copley S M 1971 *Metall. Trans.* A **2A** 215
[8] Epishin A, Link T, Portela P D and Brückner U 2000 *Acta Mater.* **48** 4169
[9] Paris O, Fährmann M, Fährmann E, Pollock T M and Fratzl P 1997 *Acta Mater.* **45** 1085–97
[10] Kostorz G 1979 *Neutron Scattering (Treatise on Materials Science and Technology)* ed G Kostorz (New York: Academic) pp 227–89
[11] Strunz P, Zrník J, Gilles R and Wiedenmann A 2000 *Physica* B **276–278** 890–1
[12] Strunz P, Šaroun J, Mikula P, Lukáš P and Eichhorn F 1997 *J. Appl. Crystallogr.* **30** 844–8
[13] Keiderling U and Wiedenmann A 1995 *Physica* B **213/214** 895–7
[14] Strunz P, Šaroun J, Keiderling U, Wiedenmann A and Przenioslo R 2000 *J. Appl. Crystallogr.* **33** 829–33
[15] Epishin A, Link T and Brückner U 2006 *Proc. 8th Liege Conf. Mater. for Advanced Power Eng.* vol 53, p 507, part 1
[16] Strunz P, Gilles R, Mukherji D and Wiedenmann A 2003 *J. Appl. Crystallogr.* **36** 854–9
[17] Press W H, Flannery B P, Teukolsky S A and Vetterling W T 1986 *Numerical Recipes* (Cambridge: Cambridge University Press)
[18] Strunz P, Mukherji D, Näth O, Gilles R and Rösler J 2006 *Physica* B **385/386** 626–9